Mesoscopic prediction on the effective thermal conductivity of unsaturated clayey soil with double porosity system

Yinkang Zhou, Changhong Yan, Anh Minh A.M. Tang, Chenglong Duan, Shengshi Dong

Mesoscopic prediction on the effective thermal conductivity of unsaturated clayey soils with double porosity system

Yinkang Zhou[a], Changhong Yan[a*], Anh Minh Tang[b], Chenglong Duan[a], Shengshi Dong[a]

[a] *School of Earth Sciences and Engineering, Nanjing University, Zhugongshan Building, Xianlin Avenue, Nanjing, Jiangsu Province 210023, PR China*

[b] *Ecole des Ponts ParisTech, 6 et 8 av. Blaise Pascal, 77455 Marne-la-Vallée, France*

Corresponding author:

Changhong Yan

Nanjing University

No.163 Xianlin Avenue, Nanjing

210023 Jiangsu Province

PR China

Email: yanchh@nju.edu.cn

Phone: +86 13952091802

Abstract: The effect of water distribution on heat conduction in unsaturated structural clayey soils with double porosity system is investigated in the present study. A dual-porosity model consisting of intra-aggregate and inter-aggregate pores is developed to describe the water distribution within intra-aggregate and inter-aggregate pores. Heat transfer using this model is then numerically simulated to determine the soil effective thermal conductivity. The obtained values are compared with available experimental data. The results show that the model can predict the accurate soil thermal conductivity values at various water contents and densities. On one hand, the model shows a higher soil thermal conductivity when water content and/or dry density are higher. On the other hand, the model shows an effect of water distribution on the soil thermal conductivity; this later is higher when water is preferentially distributed within aggregates than between aggregates. In addition, the model can give a direct visualization of heat transfer mechanisms in unsaturated clayey soils with double porosity system. In fact, heat conduction is dominant in the wet region of the dual-porosity space. This study provides both a useful predictive model of thermal conductivity and a better understanding on the physical mechanism of heat conduction in unsaturated structural clayey soils or other multiphase media with double porosity system.

Keywords: dual-porosity model; thermal conductivity; water distribution; QSGS method

1. Introduction

Thermal conductivity (λ) is one of the fundamental soil thermal properties. Understandings on soil thermal conductivity is particularly important when heat conduction process is taken into account

in a large number of geotechnical and geological applications, including energy-saving materials [1], radioactive waste disposal [2, 3], energy foundations [4-6], freezing methods [7] and moisture monitoring [8]. Soil thermal conductivity depends on numerous factors such as mineralogy, dry density, water content, temperature and microstructure, among which water content is found to be the most important factor to consider. In fact, water content is particularly important to consider in many applications because it is more likely to change appreciably in the field under changing atmospheric or boundary conditions unlike other factors (i.e. mineralogy, grain size) which remain relatively constant [9]. The influence of soil water content on thermal conductivity has been investigated extensively [3, 10-12] and a large number of models have been developed to predict soil thermal conductivity from its water content [13-16]. However, the influences of water on heat conduction are twofold: λ depends not only on the water content, but also on water distribution in soil pores [9, 17-19]. Due to the aggregation nature of fine grains, the microstructure of clayey soils is usually described as families of pores: intra-aggregate pores and inter-aggregate pores [20-23]. The presence of double porosity system results in two kinds of water defined as intra-aggregate water and inter-aggregate water. Intra-aggregate water facilitates heat conduction within aggregates by reducing thermal resistance between fine particles inside a single aggregate, while inter-aggregate water expedites heat conduction between aggregates by enhancing thermal contacts between them [21, 24]. It is thus clear that there are some differences between intra-aggregate water and inter-aggregate water in promoting heat conduction process through structural clayey soils with dual-porosity system.

The thermal conductivity of these structural soils like compacted clayey soils has been extensively

investigated [21, 24, 25], but most researches so far are based on experimental tests, which can only present an empirical relation between thermal conductivity and water contents. Experimental researches are phenomenological in nature, besides, the empirical relations between thermal conductivity and total water contents could not properly relate intra-aggregate water and inter-aggregate water to thermal conductivity and distinguish the different effects between intra-aggregate water and inter-aggregate water on heat conduction. Chen et al. [15] investigated the thermal conductivity of compacted bentonite by using Eshelby inclusion theory in mesoscale, which has obtained a series of meaningful knowledge. However, the inclusion method is limited in describing the connection between pores [26], which indeed matters in water flow in soils. Simultaneously, it might also affect heat flow process to some extent, especially for structural clayey soils with complex dual-porosity system [27, 28].

Recently, numerical simulations [29-32] on pore-scale heat conduction in porous media have been performed. Most simulations focused on the effective thermal conductivity of single-porosity media, Wang, Pan [33] developed a prevalent stochastic reconstruction approach, the Quartet Structure Generation Set (QSGS) method, to investigate the effect of particle size and water distribution on soil thermal conductivity. It is well known that clayey soils compacted on the wet side of the Optimum Water Content (OMC), i.e. at a water content higher than OMC, has a single-porosity structure[28] while it has a dual-porosity structure [34] when compacted on the dry side of OMC. Therefore, the simulations above based on QSGS method are only suitable for granular sandy soils and clayey soils compacted on the wet side of OMC rather than structural soils with dual-porosity system such as aggregated soils and clayey soils compacted on the dry

side of OMC. It is then interesting to apply dual-porosity models to simulate heat conduction when working on a predictive model for soil with dual porosity system.

In the present work, the QSGS method proposed by Wang et al. [35] is adapted to structural clayey soils with dual-porosity system. The modified model is then validated with available experimental data. That allows giving a better understanding on the heat transfer process at pore scale.

2. Numerical framework

In the present study, the integration strategy and QSGS approach are combined to investigate the thermal conductivity of structural clayey soils with dual-porosity system. QSGS method usually generates a pore-system with a uniform pore size that is manageable for single-porosity media with a relatively narrow range of pore size. Nevertheless, for dual-porosity media exhibiting different range of pore sizes at dual-scale, the QSGS method would not be appropriate. Integration strategy is quite suitable for dual-porosity media by superimposing one pore-system into another pore-system to form a combined cross-scale pore-system. An example of superposition modelling approach can also be seen in the work of Jiang et al.[36]. Hence, in the present study, the dual-porosity structure is generated by using QSGS method twice following the integration strategy. The schematic view of the method is shown in Fig. 1 and the details of this method (including 5 steps) are presented as follows.

2.1. Step 1 - Extraction of the statistical information about the pore network

To construct stochastically the pore network of dual-porosity soils, the statistical information of both inter-aggregate and intra-aggregate pores is determined in advance. The statistical information of different pores can be obtained based on the pore size distribution (PSD) curve. From the PSD curve, the density distribution of pore size can be interpreted directly by figuring out the area corresponding to the two porosity levels. This approach is easily applicable when the bi-modal shape of PSD curve is apparent [37]. The void ratio and the porosity of intra-aggregate pores are defined as e_{m} and P_{m}, while the void ratio and the porosity of inter-aggregate pores are defined as e_{M} and P_{M} (stage 1 in Fig. 1). Besides, another statistical information is about the number densities of intra-aggregate and inter-aggregate pores as well as solid particles. The physical meaning of the number density for intra-aggregate pores is that the numbers of intra-aggregate pores in a unit volume, and the same for the meaning of the number density for inter-aggregate pores and solid particles. The number densities of intra-aggregate pores, inter-aggregates pores and solid particles are named as n_{dm}, n_{dM} and n_{ds}, respectively. n_{dm} and n_{dM} can be obtained from the PSD curve as well. For a given structural clayey soil with dual-porosity system, the average volume of inter-aggregate pores is set to be v_{M} from the PSD curve. The number density of inter-aggregate pores, n_{dM}, can be derived as follows:

$$n_{\mathrm{dM}} = \frac{P_{\mathrm{M}} V}{v_{\mathrm{M}} V} = \frac{P_{\mathrm{M}}}{v_{\mathrm{M}}} \qquad (1)$$

where V is the total volume of all pores and solid particles.

The number density of intra-aggregate pores, n_{dm}, can be defined as follows:

$$n_{\mathrm{dm}} = \frac{P_{\mathrm{m}}V}{v_{\mathrm{m}}V} = \frac{P_{\mathrm{m}}}{v_{\mathrm{m}}} \quad (2)$$

where v_m is the average volume of intra-aggregate pores.

The number density of solid particles, n_{ds}, can be calculated as follows:

$$n_{\mathrm{ds}} = \frac{P_{\mathrm{s}}V}{v_{\mathrm{s}}V} = \frac{P_{\mathrm{s}}}{v_{\mathrm{s}}} \quad (3)$$

where P_s and v_s are the fraction of solid particles and the average volume of all solid particles. v_s can be reached from particle size distribution curve directly.

2.2. Step 2 - Stochastic generation of inter-aggregate pore network

In the present work, a 2D grid-system is employed to generate a pore network from the information extracted at Step 1.

Prior to generate the dual-porosity structure and water distribution by QSGS approach, the four classical parameters in QSGS approach must be introduced in advance. They are core distribution probability (C_d), directional growth probability (D_i), volume fraction (P_n) and phase interaction growth probability (I_i^{ab}). As stated by Wang, Pan [33], the core distribution probability C_d is defined as the probability of a cell in a grid system to become a core of the first growing phase. Each grid will generate automatically a random number following a uniform distribution function within (0, 1). If this number is smaller than C_d, then this grid will become the growing phase. The directional growth probability D_i is defined as the probability for a neighbor cell to become part of the growing phase in the direction i (i = 1-8; see Fig. 2). The volume fraction P_n is the proportion

of the growing phase in the grid system. If the growing phase is air, the volume fraction is usually expressed as the porosity n. The phase interaction growth probability I_i^{ab} is defined as the growing probability of a phase on b phase along the direction i. In clayey soils, due to the strong interactions between particles and bound water, the growing probability of water phase on solid phase is much larger than that of water phase on water phase along each direction.

Although the meaning of each parameter has been introduced, the relation between these parameters and the statistical properties is still unclear especially for the core distribution probabilities of inter-aggregate pores and solid particles. As stated in [38], the core distribution probability of inter-aggregate pores, C_{dM}, indicates the number density of inter-aggregate pores n_{dM}, from which C_{dM} can be defined as follows in consideration of the total number of grids, N:

$$C_{dM} = n_{dM}\frac{V}{N} \quad (4)$$

where V/N corresponds to the resolution of the grid-system.

To generate an isotropic structure in a grid system, the main directional probabilities (D_1-D_4) and the diagonal directional growth probabilities (D_5-D_8) are set to be constant: D_i = 0.0001 for i = 1-4; and D_i =0.00025 for i = 5-8, which is similar to most applications of QSGS method [33]. The QSGS approach for generating inter-aggregate pore network contains 3 sub-steps as follows (Fig. 1):

(*i*) Gas (in inter-aggregate pores) is chosen as the growing phase. The cores of gas phase are randomly located in a grid system based on the value of C_{dM}, which is the core distribution probability of the inter-aggregate pores. Each cell in the grid system is assigned with a random

number following a uniform distribution function within (0, 1). Each cell whose random number is smaller than C_{dM} is chosen as a core of gas. Note that a small value of C_{dM} will increase the random fluctuation so that the value of C_{dM} should not be too small. While *V/N* representing grid resolution should be fine enough to guarantee the precision of inter-aggregate pores, as a consequence, C_{dM} should be then small enough. In this study, C_{dM} is set as 0.001, a trade-off between random fluctuation and precise description of inter-aggregate pores.

(*ii*) All the elements of gas are enlarged to their neighboring cells in all directions based on each given directional growth probability D_i. Again, new random numbers are assigned to its neighboring cells for each gas element. The neighboring cell in direction *i* becomes a new element of gas if its random number is not greater than D_i.

(*iii*) The growing process (*ii*) is repeated until the volume fraction of gas reaches the porosity of inter-aggregate pores. Thus, the inter-aggregate pore network is constructed (Stage 2 in Fig. 1). The domain occupied by the inter-aggregate pores is defined as Ω_M, while the rest of the domain corresponds to the porous matrix representing aggregates defined as Ω_A.

2.3. Step 3 - Stochastic generation of intra-aggregate pore network

To obtain a dual-porosity network when inter-aggregate pore-system has been modeled, the intra-aggregate pores are introduced into the porous matrix for aggregates (Ω_A). Similar to the generation procedure of inter-aggregate pores, the core distribution probability of solid particles, C_{ds}, should be determined first. Noted the close relation between C_{ds} and n_{ds}, the core distribution probability of solid particles (C_{ds}) can be defined as below:

$$C_{ds} = n_{ds}\frac{V}{N(1-P_M)} \quad (5)$$

The QSGS approach adopted for generating the intra-aggregate pore network also includes 3 sub-steps (Fig. 1) as follows.

(*i*) Solid particle is chosen as the growing phase. The cores of solid phase are randomly located in the designed porous matrix region (Ω_A) above based on the value of Cd_S. Each cell in Ω_A is assigned a random number following a uniform distribution function within (0, 1). Each cell whose random number is not greater than Cd_S is chosen as a core of solid particle. While, in clayey soils, the average size of solid particles is much smaller than that of inter-aggregate pores, so the number density of particles is greater than that of inter-aggregate pores in a unit volume, which results in the core distribution probability of solid particles is always much higher and set as 0.1 or 0.2 in the present study.

(*ii*) Every element of solid is enlarged to its neighboring cells in all directions. For each solid element, new random numbers are assigned to its neighboring cells. The neighboring cell in direction *i* will become a new element of solid phase if its random number is smaller than D_i.

(*iii*) The growing process (*ii*) is repeated until the volume fraction of solid particles reaches the value extracted at Step 1 (Stage 3 in Fig. 1). The domain occupied by the intra-aggregate pores is defined as Ω_m, while the rest of the domain corresponds to the solid particles.

2.4 Step 4 - Distribution of water in the pore network

The water phase grows following the phase interaction growth probability I_i^{ws} and I_i^{ww}; I_i^{ws} represents the growth probability of the water phase on the solid phase along direction *i*, and I_i^{ww} represents the growth probability of the water phase on the water phase along direction *i*. In this

study, clayey soils are investigated. It is well known that clay particles have a strong water adsorption capacity and water would exist in the form of liquid-film on the clay particle surface in spite of intra-aggregate water and inter-aggregate water. Besides, it is very difficult to distinguish the different morphologies of water-film for these two kinds of water, and there has not been a clear data for this issue. Therefore, these two types of water-film are set to be similar to simplify analysis. Then to model such a water-film, I_i^{ws} has been set ten times larger than I_i^{ww} as used by Wang et al. [38]. Furthermore, the water growth phase is first started in the domain of intra-aggregate pore Ω_m, when the volume of water is higher than the volume of intra-aggregate pore, the inter-aggregate pores start to be filled with water (stage 4 in Fig. 1).

2.5. Step 5 - Determination of the effective thermal conductivity

Figure 3 shows an example of the three-phase medium generated following the above steps. To determine the effective thermal conductivity of this medium, thermal boundary conditions are imposed as shown in Fig. 3. Constant temperatures are imposed on the left and right sides while adiabatic conditions are imposed on the top and bottom sides.

In 1-D heat conduction condition, heat flow between two cell *i* and *j* is calculated as follows:

$$q_{ij} = \lambda_{ij} \frac{T_i - T_j}{L_{ij}} \quad (6)$$

where q_{ij} and L_{ij} are the heat flux density and the distance between the two cells *i* and *j*, and the temperatures in the center of cells *i* and *j* are T_i and T_j, respectively. λ_{ij} denotes the effective thermal conductivity between two neighbor cells. Each cell contains only one phase and λ_{ij} is calculated by the harmonic mean method [39].

When the steady state is reached, the heat flux density through each cell in the computational region keeps balanced, which can be described as below.

$$\sum_i q_{ij} = 0 \qquad (7)$$

Based on the analyses above, the discrete equations about the temperature can be obtained by integrating the governing Eq. (7) over all the cells in the computational region. Consequently, when the number of cells in which the temperature is unknown is *X*, and there will be an equal number of linear equations to solve the temperature field. As long as the temperature field is determined, the effective thermal conductivity can be calculated by the following formula:

$$\lambda = \frac{L \times \int q dx}{T_h - T_c} \qquad (8)$$

where q is the steady heat flux density through each cell along the y direction and L is the distance width of the grid (see Fig. 3).

In the present work, a square grid is used with the same number of cells on the x and the y direction. A preliminary work has been done to optimize the grid dimension. In Fig. 4, the thermal conductivity of the medium is plotted versus the grid dimension. The results show that the effective thermal conductivity of the medium becomes independent of the grid dimension when the latter is higher than 200 cells. Hence, in the present study, a grid system of 200×200 cells is used for all the simulations. As shown in Fig. 3, this system allows to represent several large pores with diameters of approximately 50 cells.

3. Results

3.1 Validation

To validate the approach proposed in this study for calculating the effective thermal conductivity of structural clayey soils with dual-porosity system, the numerical results are compared with experimental data [3, 24] from literatures in this section.

In the work of Tang et al. [3], MX80 bentonite, containing 92% of montmorillonite, from Wyoming (being considered as a potential reference buffer material for high-level radioactive waste disposal in several countries) was compacted at various water contents (w = 9% for series S1; 11.7% for S2; and 17.9% for S3). Each series includes several specimens compacted at various dry densities. Besides, some compacted specimens of series S2 were dried to obtain a water content of 9.1% (series S2b), and the series S3b corresponds to specimens of series S3 dried to a water content of 10.2%. Tang et al. [3]expected that compacted specimens prepared with direct compaction and with drying after compaction would have different moisture distribution in the pore space. The thermal conductivity of compacted soil specimens was measured by a commercial thermal properties analyser, KD2 (Decagon Devices Inc.) based on the hot wire method.

The porosity of intra-aggregate pores is determined as follows for each water content. The soil suction at each water content is estimated from the water retention curve [40], then e_m is determined from the relation between e_m and suction [23]. Noted that e_m increases as water content increases due to the expansion of aggregates and e_M decreases as dry density increases, and the values of void ratio corresponding to these intra-aggregate pores (e_m) are shown in Table 1. The

thermal conductivity of water and gas are taken as λ_w =0.5974 W/m·K, λ_g=0.0243 W/m·K, and the thermal conductivity of solid phase λ_s (which depends on the soil mineralogy) is equal to 2.0825 W/m·K following the study of Tang et al. [3].

Figure 5 shows the experimental results of the compacted samples and those obtained by the model. In Fig. 6, the predicted thermal conductivities are plotted versus the measured values for all the samples. The results show that the model can predict the accurate thermal conductivity values of samples subjected to drying path while it overestimates those of samples obtained by direct compaction.

Different preparation methods may result in different water distribution states. For the samples obtained by compaction, they would contain water both within and between aggregates[41]. However, for samples prepared by drying, both intra-aggregate water content and inter-aggregate water content are unknown, more water would be preferentially stored in intra-aggregate pores. Hence, the present model (where water was preferentially distributed in intra-aggregate pores) can predict the accurate thermal conductivity values of samples obtained by drying due to the reasonable model of water distribution. In order to have a deeper analysis on the effect of water, a complementary model (Model 2) is employed where water is distributed preferentially in inter-aggregate pores.

To evaluate this assumption, the experimental results of all samples obtained by compaction are compared against their corresponding predictions by the two models in Fig. 7. In this figure, the

291 results obtained by the two models are plotted in the form of error bars. The upper bound
292 corresponds to the water distributed preferentially in intra-aggregate pores (Model 1) and the
293 lower bound corresponds to the water distributed preferentially in inter-aggregate pores (Model 2).
294 It can be seen from Fig. 7 that the experimental results of series S1 mainly correspond to the lower
295 bound of the model, while those of the series S2 fall in the range between the lower and the upper
296 bounds. However, only the result of one sample in the series S3 (with lowest dry density) agrees
297 with the model, and those of the two others are over-predicted.
298
299 In the study of Usowicz et al. [24], a haplic phaeozem at Werbkowice was sieved into six series
300 and each one has different aggregate sizes. The soil aggregates in each series were loosely packed
301 into the cylinders of 100 cm^3 volume, 5 cm diameter in five replicates. Some characteristics of the
302 soil were given in Table 2 [42, 43], and the method for measuring thermal conductivity was also
303 taken from Sikoro [43].
304
305 The influence of volumetric water content on the thermal conductivity in structural clayey soil was
306 also investigated at various aggregate sizes. The pore size distribution of soil samples was not
307 available. The porosity of intra-aggregate pores was then determined following the suggestion of
308 Real et al.[44]. They measured the thermal conductivity of structural lightweight aggregate
309 concrete at various water contents. The results show an inflection point in the relation between
310 thermal conductivity and water content. That point corresponds to the transition from
311 inter-aggregate water to intra-aggregate water at a drying path. Thus, the water content at the
312 inflection point can be used to estimate the porosity of intra-aggregate pores. In the work of

313 Usowicz et al. [24], all curves presented an inflection point at a volumetric water content of 20%.
314 In the present work, the porosity of intra-aggregate pores was then estimated to be 0.20.
315
316 Figure 8 presents the experimental data and the predicted results of the samples with different
317 aggregate sizes. Figure 9 shows the thermal conductivity predicted by the model versus the
318 experimental data. In Table 3, the summary statistics of measured and predicted thermal
319 conductivities are compared between the present study and the study of Usowicz et al. [24].
320
321 Figure 8 shows that the model can predict the accurate thermal conductivity values for most of the
322 experimental data except that with aggregate size smaller than 0.25 mm. In fact, the latter
323 corresponds to non-aggregated soil sample, which means it does not have a dual-porosity system.
324 Table 3 shows that the model in the present study can improve the prediction as compared to the
325 one proposed by Usowicz et al. [24]; its coefficient of determination R^2 is higher than that of
326 Usowicz et al. [24] for all the series of soil samples, except that with aggregate size smaller than
327 0.25 mm.

328 ## 3.2. Pore-scale heat flow analysis

329 A series of typical heat flow density fields are required to give a deep insight into how heat
330 transfers within and between aggregates in structural clayey soils with dual-porosity system. Three
331 typical water distribution model in the dual-porosity space and their corresponding heat flow
332 density fields at different water contents are chosen for comparison to give a visual presentation
333 about the heat flow path and its relation with water distribution. In Fig. 10, the pure structural

model of the dual-porosity system without any water (e_w=0) is presented in the top, below which its corresponding heat flow density field is shown. The second water content corresponds to the content with saturated intra-aggregate pores (e_w=e_m), the structural model of water distribution is shown as the upper half in Fig. 11 and the corresponding heat flow density field as the lower half. As to the third water content, it is set to be twice of the water content of the second one (e_w=2e_m). Simultaneously, their water distribution and heat flow density field are shown in Fig. 12 with a similar layout in Figs. 10 and 11.

From Figs. 10, 11 and 12, we can see that heat flow mainly goes through connected aggregated generally. In addition, it is preferred to the wet region in the dual-porosity space. It is thus clear that heat conduction is closely dependent on the water distribution between intra-aggregate pores and inter-aggregate pores. With the increase of water content, water is mostly retained within aggregates. Heat flow path mainly falls within the region of aggregates and none flow path pass through the areas of inter-aggregate pores. As the water content continues to increase, intra-aggregate pores are saturated and water appears in inter-aggregate pores in form of liquid-film along the aggregates region. In this case, heat flow path is getting wider and wider, and the added region for the path just corresponds to the space occupied by the inter-aggregate water in this stage. It can be clearly observed that there is a difference in widening heat flow paths between intra-aggregate water and inter-aggregate water. Intra-aggregate water mainly widens heat flow between fine particles within aggregates, while inter-aggregate water mainly acts on broaden heat flow path in the inter-aggregate pores. Except for a correct prediction of effective thermal conductivity, this model can also directly show how heat transfers in soils at pore scale.

The latter can be seen as another promising advantage of the model, especially for the differences in promoting heat conduction between intra-aggregate water and inter-aggregate water from a perspective of heat flow paths.

4 Discussions

Microstructural-based quantitative computation of the thermal conductivity in structural clayey soils is always challenging due to the presence of dual-porosity system. As a promising tool to relate structural properties to thermal conductivity in porous media, numerical modelling has been employed in this field. But less effort was made to model heat transfer process in complex dual-porosity media [45] like compacted clayey soils. Dong et al. [46] presented a critical review on the models for predicting soil thermal conductivity and classified the models into three types including mixing models, empirical models and mathematical models. For examples, the most popular Johansen model [13] belongs to the empirical models. In most of these models, the effect of water distribution on thermal conductivity is ignored. In the present work, as the water distribution is considered, simulations show clearly that heat transfer is controlled by thermal contacts between aggregates and inside the aggregates. These domains are strongly influenced by the presence of inter-aggregate water and intra-aggregate water.

It should be noted that the model could predict the accurate thermal conductivity values when the dual-porosity system of the soil pore network is dominant. In the case of soil compacted at high densities (or compacted on the wet side of OMC), the volume of inter-aggregate pore is negligible.

In these cases, the accuracy of the predictive model would be adversely affected and it tends to overestimate the values of soil thermal conductivity (see Fig. 7). This problem would be improved by generating a more realistic pore network [47] but it would be more time consuming.

It is thus clear that the proposed model in this paper is still far away from a mature predictive model, and it would be a long way to go as a new predictive one compared with other experienced models. In addition to the accuracy problem, some other limitations are also noteworthy. Soil structure is three-dimensional, heat conduction process in real soils is much more complex while the predictive model in our work is a 2-D model and would be somewhat inadequate to provide a more detailed description. Furthermore, as a new predictive model, it still needs to be validated by more experimental data with both thermal conductivity values and pore size distribution curves available. Finally, yet importantly, the determination of the Representative Element Volume (REV) and its mesh need more considerations. The size of the REV should be large enough to avoid random fluctuation, at the same time the mesh size should be small enough to guarantee a precise description of the fine pores. The cost for modeling would be extremely high if the above demands are both satisfied, under this circumstance, an in-depth trade-off must be carried out to make minor sacrifices to safeguard the major interests. In the present study, the grid dimension strategy is just a simple case and more work is needed to give more insights into this issue. In addition, it should be noted that the present model only describes heat transfer by conduction process in unsaturated soils, and other phenomenon such as latent heat transfer is ignored. It has been experimentally shown [48] that heat transfer is dominant by conduction for unsaturated soils in a low-temperature range (2℃ to 30℃), while latent heat transfer turns out to be noticeable when

399 the temperature is high enough (greater than 40℃) in soils. Hence, the present model is then
400 mostly suitable over a low-temperature range.
401
402 The effect of water distribution on soil properties is usually related to hysteresis effect. For
403 compacted clayey soils as a typical case, Tang et al. [3] found that the thermal conductivity of
404 specimens obtained by drying was higher than that of specimens prepared by direct compaction
405 with the same dry density and water content. This phenomenon was also noted by Farouki [11]. In
406 compacted soils with dual-porosity system, water distribution depends largely on
407 hydro-mechanical history. It is well known that at a given water content the matric suction on a
408 drying path (or a unloading path) is always higher than that on a wetting path (a loading path).
409 Indeed, matric suction indicates water distribution state; higher suction means that more water
410 tends to be retained in intra-aggregate pores with small pore size. For this reason, there is more
411 water distributed within aggregates for specimens obtained by drying than that for the specimens
412 obtained by compaction in the study of Tang et al.[3]. This effect of water distribution on soil
413 thermal conductivity is demonstrated by the simulations obtained by the present model. In
414 addition, it should be noted that when the soil pore network is dominated by a monomodal
415 porosity, the hysteresis effect on thermal conductivity would be negligible. Nguyen et al. [49]
416 investigated thermal conductivity of natural loess during wetting-drying paths, whose pore size
417 distribution shows only one pore family, and they found a unique relationship between thermal
418 conductivity and degrees of saturation.
419

5. Conclusions

In the present work, the thermal conductivity of structural clayey soils with dual-porosity system is predicted based on its microstructure and water distribution. The following conclusions can be drawn:

1) A microstructural-based model is proposed to calculate thermal conductivity of structural clayey soils with dual-porosity system. The model was validated with the data obtained from two types of soils. The results show that the model can give appropriate predictions when the dual porosity system is dominant in the soil pore network.
2) Water distribution has a significant effect on soil thermal conductivity. Thermal conductivity is always higher when water is preferentially distributed within aggregates than between aggregates.
3) The model can give a deep insight into heat flow paths at pore scale. Numerical simulations demonstrate that heat conduction mainly goes through aggregate region and is preferred to wet pores of the dual-porosity space.

Acknowledgement

We would like to thank Xianqiang Meng and Shaohua Cao for helpful discussions and Huanran Wu for editing the text.

Reference

1. Khedari, J., B. Suttisonk, N. Pratinthong, and J. Hirunlabh, *New lightweight composite construction materials with low thermal conductivity.* Cement & Concrete Composites, 2001. **23**(1): p. 65-70.
2. Ould-Lahoucine, C., H. Sakashita, and T. Kumada, *Measurement of thermal conductivity of buffer materials and evaluation of existing correlations predicting it.* Nuclear Engineering & Design, 2002. **216**(1): p. 1-11.
3. Tang, A.-M., Y.-J. Cui, and T.-T. Le, *A study on the thermal conductivity of compacted bentonites.* Applied Clay Science, 2008. **41**(3-4): p. 181-189.
4. Abdelaziz, S.L., C.G. Olgun, and J.R. Martin, *Counterbalancing ambient interference on thermal conductivity tests for energy piles.* Geothermics, 2015. **56**: p. 45-59.
5. Brettmann, T. and T. Amis, *Thermal Conductivity Evaluation of a Pile Group Using Geothermal Energy Piles.* 2011: p. 499-508.
6. Vijdea, A.-M., C. Weindl, A. Cosac, N.-S. Asimopolos, and D. Bertermann, *Estimating the thermal properties of soils and soft rocks for ground source heat pumps installation in Constanta county, Romania.* Journal of Thermal Analysis and Calorimetry, 2014. **118**(2): p. 1135-1144.
7. Zhou, J. and Y. Tang, *Centrifuge experimental study of thaw settlement characteristics of mucky clay after artificial ground freezing.* Engineering Geology, 2015. **190**: p. 98-108.
8. Cao, D., B. Shi, S.P.L. Ii, X. Gong, H.H. Zhu, G. Wei, and L. Yang, *Investigation of the influence of soil moisture on thermal response tests using active distributed temperature sensing (A–DTS) technology.* Energy & Buildings, 2018.
9. Likos, W.J., *Pore-Scale Model for Thermal Conductivity of Unsaturated Sand.* Geotechnical and Geological Engineering, 2014. **33**(2): p. 179-192.
10. Kersten, M.S., *Laboratory research for the determination of the thermal properties of soil.* Journal of Neurophysiology, 1949. **45**(4): p. 667-697.
11. Farouki, O., *Thermal Properties of Soils, Series on Rock and Soil Mechanics.* 1986.
12. Tarnawski, V.R. and W.H. Leong, *Thermal Conductivity of Soils at Very Low Moisture Content and Moderate Temperatures.* Transport in Porous Media, 2000. **41**(2): p. 137-147.
13. Johansen, O., *Thermal conductivity of soils* 1975, Trondheim Norway.
14. Côté, J. and J.-M. Konrad, *A generalized thermal conductivity model for soils and construction materials.* Canadian Geotechnical Journal, 2005. **42**(2): p. 443-458.
15. Chen, Y., S. Zhou, R. Hu, and C. Zhou, *A homogenization-based model for estimating effective thermal conductivity of unsaturated compacted bentonites.* International Journal of Heat & Mass Transfer, 2015. **83**: p. 731-740.
16. Chen, Y., S. Zhou, R. Hu, and C. Zhou, *Estimating effective thermal conductivity of unsaturated bentonites with consideration of coupled thermo-hydro-mechanical effects.* International Journal of Heat and Mass Transfer, 2014. **72**: p. 656-667.
17. Dong, Y. and S. Pamukcu, *Thermal and electrical conduction in unsaturated sand controlled by surface wettability.* Acta Geotechnica, 2014. **10**(6): p. 821-829.
18. Kim, D., G. Kim, and H. Baek, *Relationship between thermal conductivity and soil–water characteristic curve of pure bentonite-based grout.* International Journal of Heat and Mass Transfer, 2015. **84**: p. 1049-1055.

19. Likos, W.J., *Modeling Thermal Conductivity Dryout Curves from Soil-Water Characteristic Curves.* Journal of Geotechnical & Geoenvironmental Engineering, 2013. **140**(5): p. 04013056.
20. Salla, S., S. Outi, T.E. Strandberg, K. Pentti, A.Y. Strandberg, R.S. Tilvis, K.H. Pitk?L?, T.A. Miettinen, and F. Frej, *Use of mercury intrusion porosimetry for microstructural investigation of reconstituted clays at high water contents.* Engineering Geology, 2013. **158**(3): p. 15-22.
21. Ju, Z., T. Ren, and C. Hu, *Soil Thermal Conductivity as Influenced by Aggregation at Intermediate Water Contents.* Soil Science Society of America Journal, 2011. **75**(1): p. 26.
22. Romero, E., G. Della Vecchia, and C. Jommi, *An insight into the water retention properties of compacted clayey soils.* Géotechnique, 2011. **61**(4): p. 313-328.
23. Tang, A.M. and Y.J. Cui, *Modelling the thermo-mechanical volume change behaviour of compacted expansive clays.* Géotechnique, 2009. **59**(3): p. 185-195.
24. Usowicz, B., J. Lipiec, J.B. Usowicz, and W. Marczewski, *Effects of aggregate size on soil thermal conductivity: Comparison of measured and model-predicted data.* International Journal of Heat and Mass Transfer, 2013. **57**(2): p. 536-541.
25. Hadas, A., *Heat Transfer in Dry Aggregated Soil: I. Heat Conduction.* Soil Science Society of America Journal, 1977. **41**(6): p. 1055-1059.
26. Chen, Y., S. Hu, C. Zhou, and L. Jing, *Micromechanical Modeling of Anisotropic Damage-Induced Permeability Variation in Crystalline Rocks.* Rock Mechanics and Rock Engineering, 2013. **47**(5): p. 1775-1791.
27. Carson, J.K., S.J. Lovatt, D.J. Tanner, and A.C. Cleland, *An analysis of the influence of material structure on the effective thermal conductivity of theoretical porous materials using finite element simulations.* International Journal of Refrigeration, 2003. **26**(8): p. 873-880.
28. Wang, Y., Y.J. Cui, A.M. Tang, C.S. Tang, and N. Benahmed, *Changes in thermal conductivity, suction and microstructure of a compacted lime-treated silty soil during curing.* Engineering Geology, 2016. **202**: p. 114-121.
29. Wang, M. and N. Pan, *Modeling and prediction of the effective thermal conductivity of random open-cell porous foams.* International Journal of Heat and Mass Transfer, 2008. **51**(5-6): p. 1325-1331.
30. Zhang, H., X. Ge, and H. Ye, *Randomly mixed model for predicting the effective thermal conductivity of moist porous media.* Journal of Physics D: Applied Physics, 2006. **39**(1): p. 220-226.
31. Wang, D., Z. Liu, J. Shen, and W. Liu, *Lattice Boltzmann Simulation of Effective Thermal Conductivity of Porous Media with Multiphase.* Journal of Porous Media, 2015. **18**(10): p. 929-939.
32. Albert, K., C. Franz, R. Koenigsdorff, and Z. Kai, *Inverse estimation of rock thermal conductivity based on numerical microscale modeling from sandstone thin sections.* Engineering Geology, 2017. **231**.
33. Wang, M., N. Pan, J. Wang, and S. Chen, *Mesoscopic simulations of phase distribution effects on the effective thermal conductivity of microgranular porous media.* J Colloid Interface Sci, 2007. **311**(2): p. 562-70.
34. Delage, P., M. Audiguier, Y.J. Cui, and M.D. Howat, *Microstructure of a compacted silt.* Canadian Geotechnical Journal, 1996. **33**(1): p. 150-158.
35. Wang, M., J. Wang, N. Pan, and S. Chen, *Mesoscopic predictions of the effective thermal*

conductivity for microscale random porous media. Phys Rev E Stat Nonlin Soft Matter Phys, 2007. **75**(3 Pt 2): p. 036702.
36. Jiang, Z., M.I.J. van Dijke, K.S. Sorbie, and G.D. Couples, *Representation of multiscale heterogeneity via multiscale pore networks.* Water Resources Research, 2013. **49**(9): p. 5437-5449.
37. Pinyol, N.M., A. Gens, and E.E. Alonso, *Compacted soil behaviour: initial state, structure and constitutive modelling.* Geotechnique, 2013. **63**(6): p. 463-478.
38. Wang, M. and N. Pan, *Predictions of effective physical properties of complex multiphase materials.* Materials Science and Engineering: R: Reports, 2008. **63**(1): p. 1-30.
39. Huai, X., W. Wang, and Z. Li, *Analysis of the effective thermal conductivity of fractal porous media.* Applied Thermal Engineering, 2007. **27**(17–18): p. 2815-2821.
40. Tang, A.M. and Y.J. Cui, *Controlling suction by the vapour equilibrium technique at different t.* Canadian Geotechnical Journal, 2005. **42**(1): p. págs. 287-296.
41. Delage, P., D. Marcial, Y.J. Cui, and X. Ruiz, *Ageing effects in a compacted bentonite: a microstructure approach.* Geotechnique, 2006. **56**(5): p. 291-304.
42. Witkowska, B., *The impact of aggregate structure of mineral soils on their hydrophysical characteristics.* 2000.
43. Sikora, E., *Thermal properties of aggregate soil samples for different aggregate diameter and moisture*. 1983, Agricultural Univesity,Lubin, Poland. p. 106.
44. Real, S., J.A. Bogas, M.D.G. Gomes, and B. Ferrer, *Thermal conductivity of structural lightweight aggregate concrete.* Magazine of Concrete Research, 2016: p. 1-11.
45. Heinze, T. and S. Hamidi, *Heat transfer and parameterization in local thermal non-equilibrium for dual porosity continua.* Applied Thermal Engineering, 2017. **114**: p. 645-652.
46. Dong, Y., J.S. McCartney, and N. Lu, *Critical Review of Thermal Conductivity Models for Unsaturated Soils.* Geotechnical and Geological Engineering, 2015. **33**(2): p. 207-221.
47. Zhao, T., H. Zhao, Z. Ning, X. Li, and Q. Wang, *Permeability prediction of numerical reconstructed multiscale tight porous media using the representative elementary volume scale lattice Boltzmann method.* International Journal of Heat & Mass Transfer, 2018. **118**: p. 368-377.
48. Nikolaev, V. Ivan, Leong, H. Wey, Rosen, and A. Marc, *Experimental Investigation of Soil Thermal Conductivity Over a Wide;Temperature Range.* International Journal of Thermophysics, 2013. **34**(6): p. 1110-1129.
49. Nguyen, V.T., H. Heindl, J.M. Pereira, A.M. Tang, and J.D. Frost, *Water retention and thermal conductivity of a natural unsaturated loess.* Géotechnique Letters, 2018. **7**(4): p. 1-6.

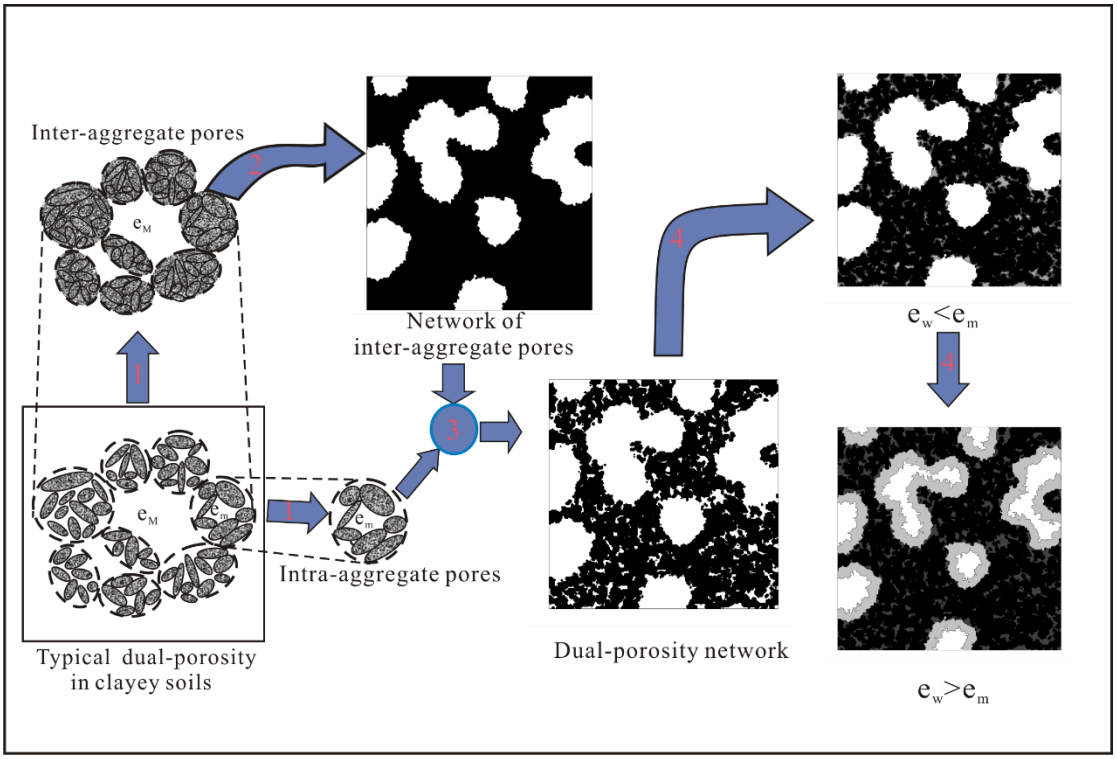

566

567 Fig. 1. Workflow to generate dual-porosity network and water distribution: (1) extraction of e_m and

568 e_M; (2) generation of inter-aggregate pores; (3) generation of intra-aggregate pores, (4) water

569 distribution within aggregates and between aggregates.

570

571

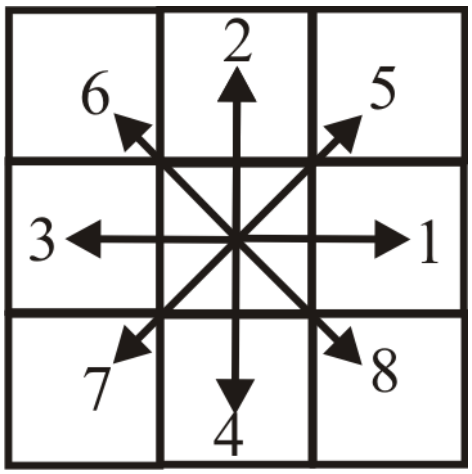

572

573 Fig. 2. Growth directions of each cell to its neighbor cells.

574

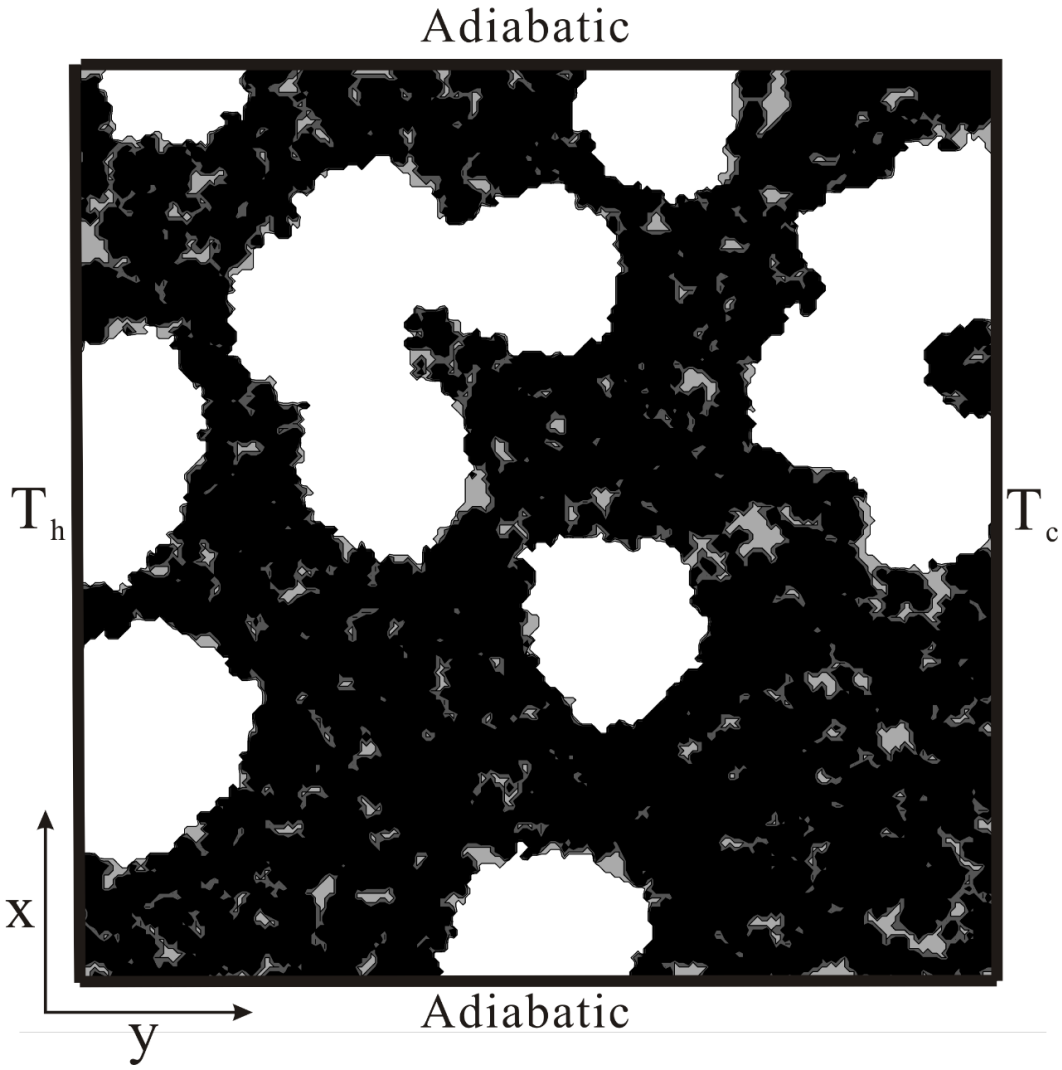

575

576 Fig. 3. Schematic view of the computational domain and the boundaries.

577

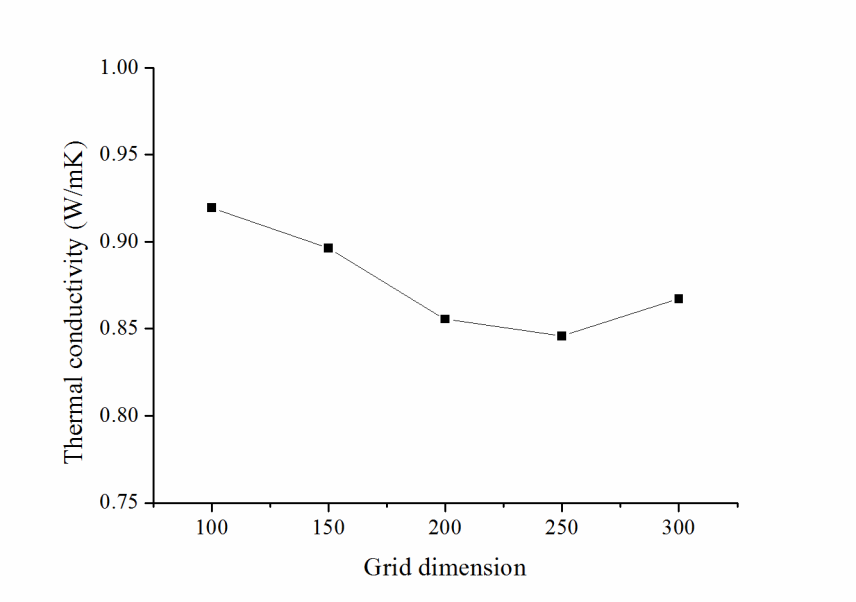

578

579 Fig. 4. Thermal conductivity versus grid dimension.

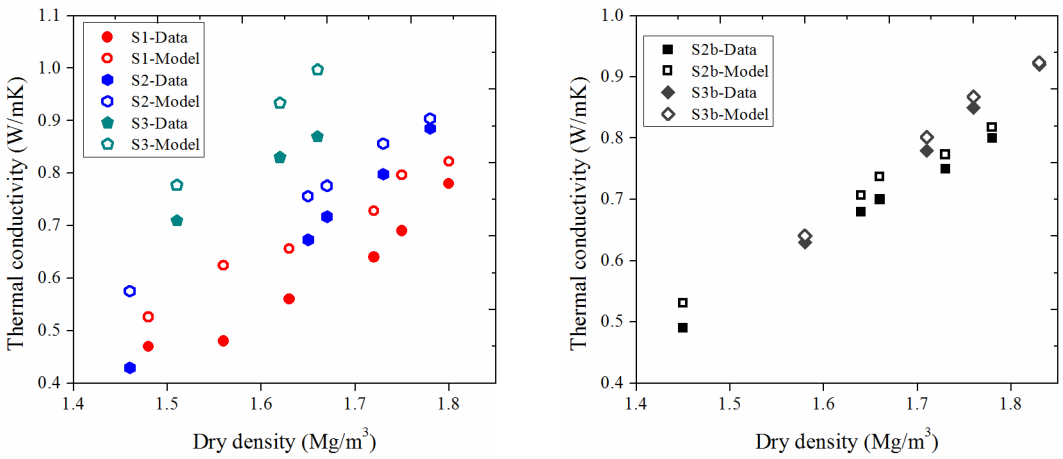

(a) (b)

580 Fig. 5. Thermal conductivity of samples obtained by compaction (a) and obtained by drying (b) for

581 samples from Tang et al. [3].

582

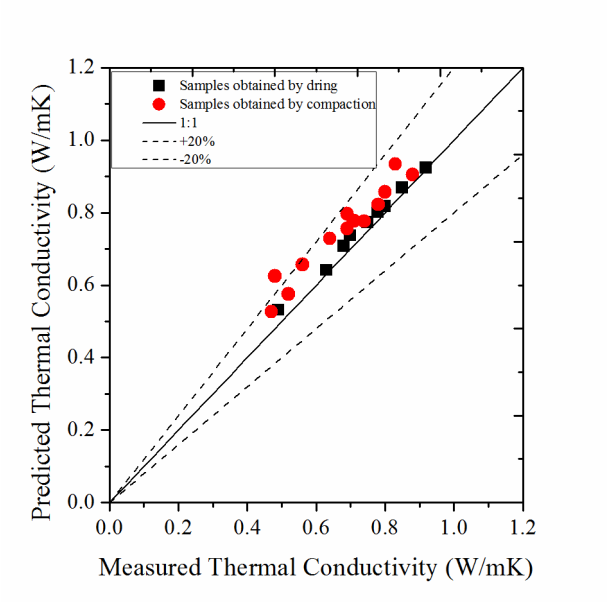

583

584 Fig. 6. Predicted thermal conductivity versus measured ones for samples from Tang et al. [3].

585

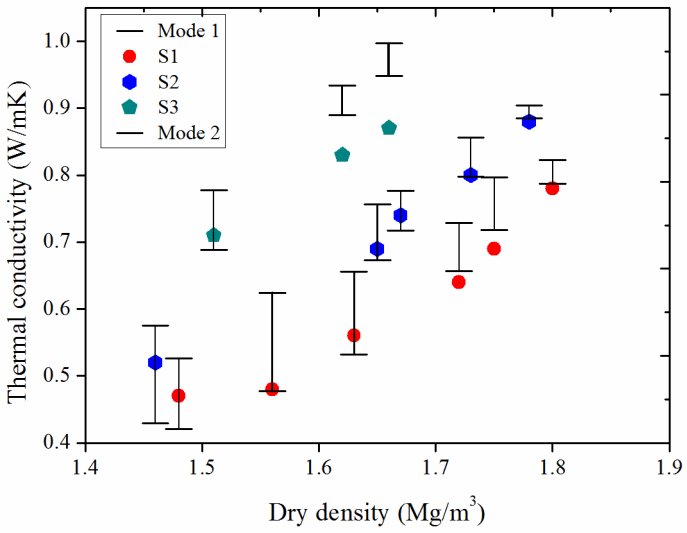

586

587 Fig. 7. Thermal conductivity versus dry density for samples from Tang et al. [3]: experimental data

588 and the two models.

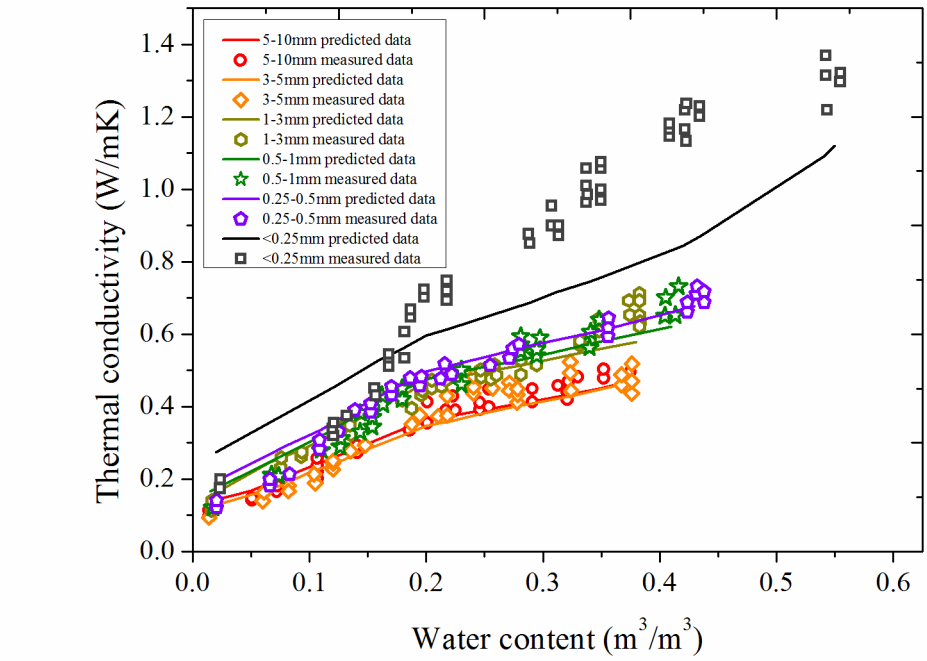

589

590 Fig. 8. Experimental data and modelled results of different aggregate size in Usowicz et al. [24].

591

592

593

594

595

596

597

598

599

600

601

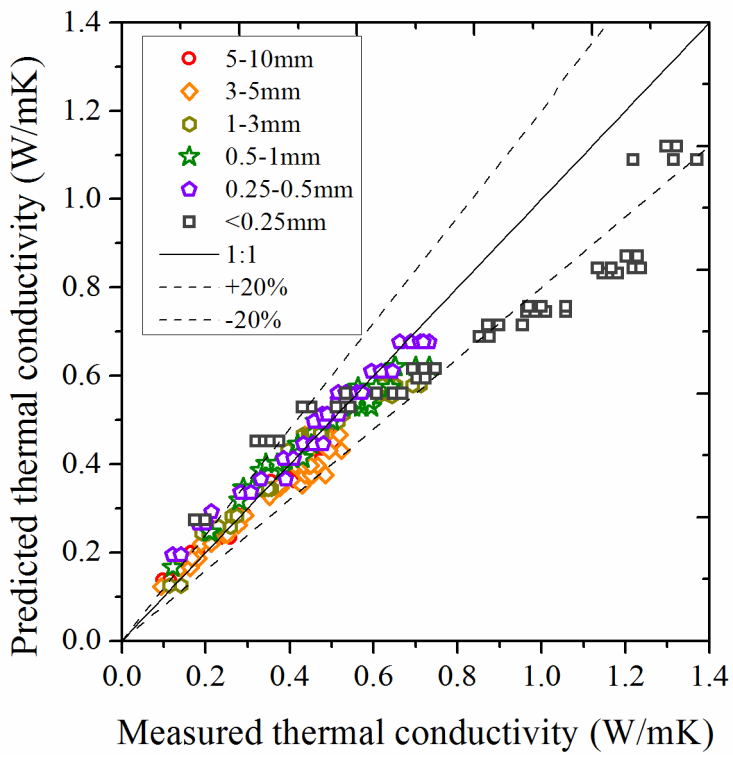

602

603 Fig. 9. Modelled results by mode 1versus experimental data in Usowicz et al. [24].

604

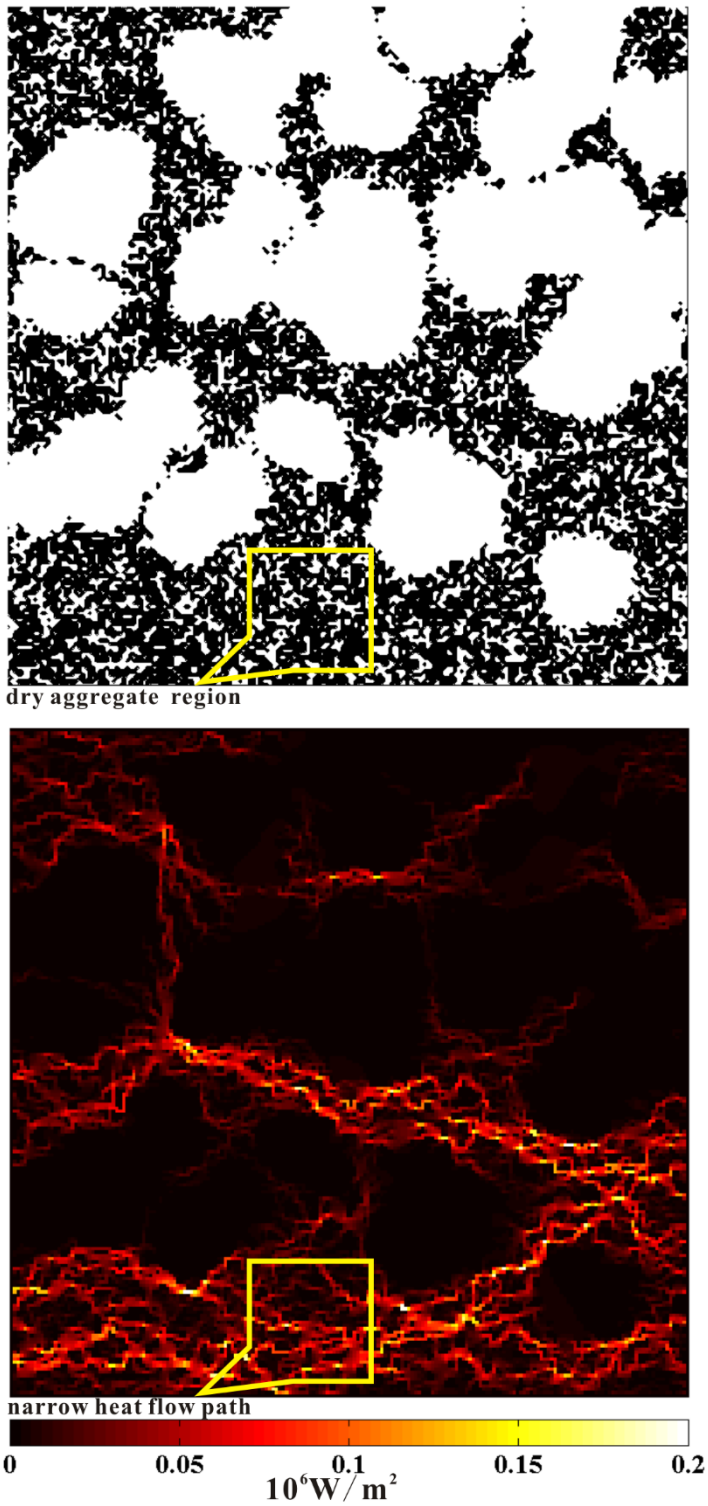

Fig. 10. Multi-phase distribution at the first water content (e_w= 0) in the upper half and its corresponding heat flux density field in the lower half.

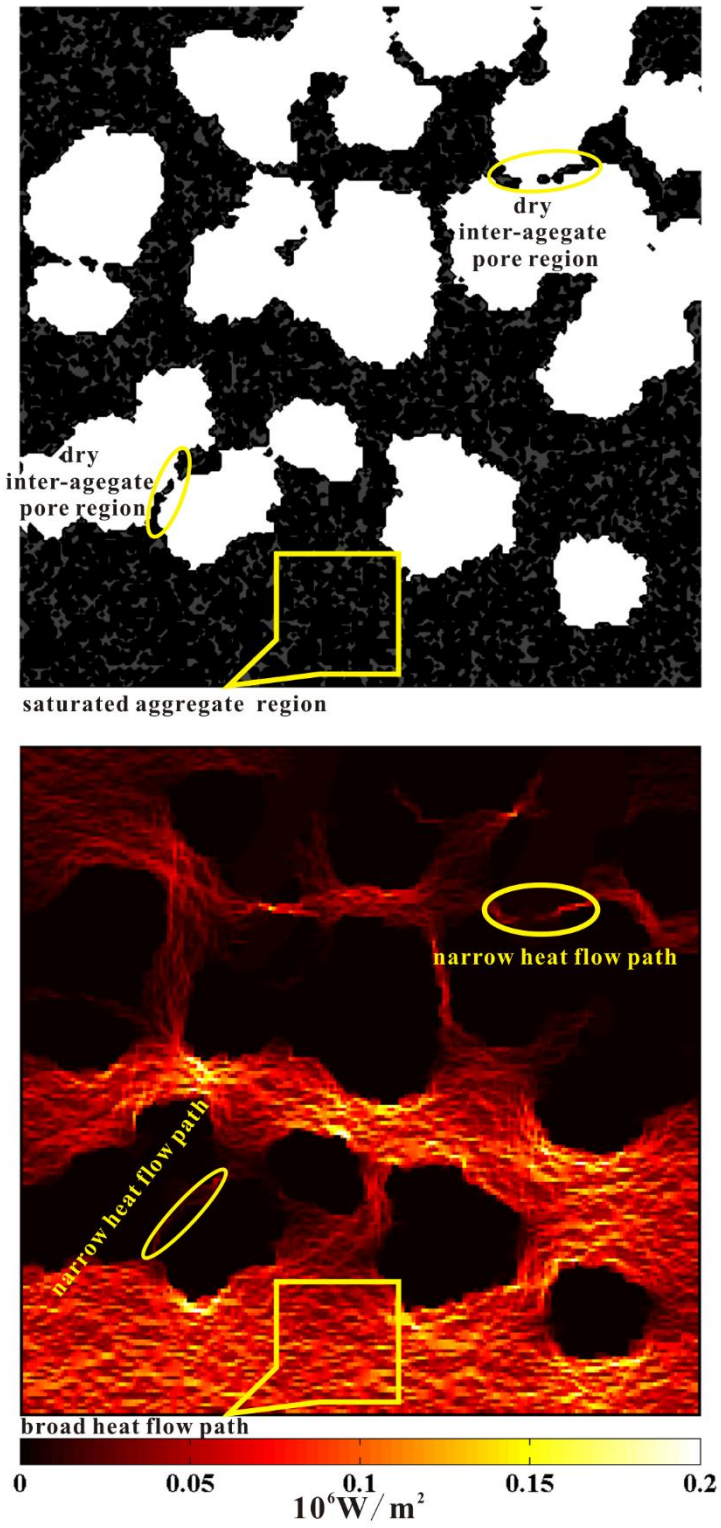

610

611 Fig. 11. Multi-phase distribution at the second water content (e_w=e_m) in the upper half and its

612 corresponding heat flux density field in the lower half.

613

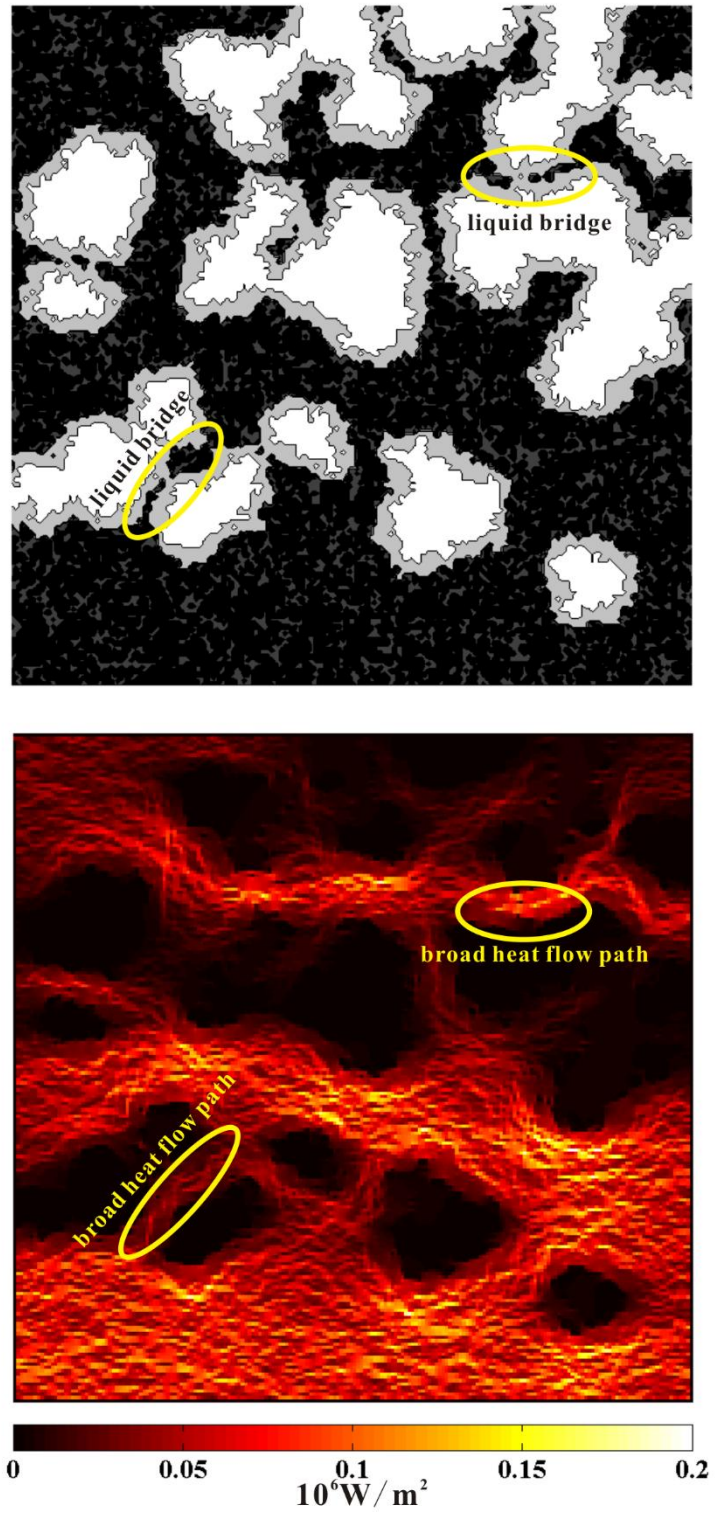

Fig. 12. Multi-phase distribution at the third water content (e_w=2e_m) in the upper half and its corresponding heat flux density field in the lower half.

Table 1 Detailed e_m and e_w information at each water content in [3].

w (%)	9.0(S1)	9.1(S2b)	10.2(S3b)	11.7(S2)	17.9(S3)
e_m	0.43	0.43	0.46	0.50	0.58
e_w	0.25	0.25	0.28	0.32	0.49

Table 2 Characteristics of the Haplic Phaeozem at Werbkowice.

Aggregate size (mm)	Particle size (mm) distribution (%,w/w)			Organic matter contents (%)	Bulk density(Mg cm^{-3})	Porosity(m^{-3} m^{-3})
	1.0-0.10	0.1-0.02	<0.02			
All	3	57	40	2.18	1.09	0.59
<0.25	3	61	36	3.38	1.18	0.55
0.25-0.5	4	52	44	4.61	0.98	0.64
0.5-1	4	53	43	4.37	0.89	0.66
1-3	3	55	42	4.55	0.94	0.65
3-5	5	52	43	4.37	0.83	0.69
5-10	3	53	44	4.13	0.84	0.68

628

629 Table 3 Comparison of statistics between this study (left) and [24](right).

Aggregate size (mm)	5-10		3-5		1-3		0.5-1		0.25-0.5		<0.25	
Linear regression coefficient	0.823	1.458	0.783	1.394	0.794	1.560	0.741	1.520	0.834	1.561	0.580	1.088
Intercept	0.053	-0.158	0.053	-0.145	0.082	-0.198	0.117	-0.209	0.093	-0.232	0.208	-0.043
Coefficient of determination R^2	0.976	0.859	0.937	0.810	0.950	0.938	0.964	0.932	0.978	0.925	0.911	0.978

630

631

632